Aust. J. Phys., 1987, **40**, 619–34

Correlations in Space and Time for a Soft-mode Phase-transforming System

S. L. Mair

Division of Materials Science and Technology, CSIRO,
Locked Mail Bag 33, Clayton, Vic. 3168, Australia.

Abstract

Using molecular dynamics (MD) for a system of nonlinear (quadruple-quadratic) oscillators on a nearest-neighbour square lattice, the pair-displacement correlations and the frequency spectrum for the dynamical order-parameter correlation function are obtained as a function of temperature. For temperatures T near T_c, the pair-displacement correlation function (with the long-range order component subtracted out) was found to vary with particle separation r as $r^{-1/2}\exp\{-\lambda(T)r\}$, at least out to the tenth neighbour in the 40×40 particle lattice. This is consistent with predictions for the two-dimensional Ising model for T above, but not below, T_c. The frequency spectrum for the dynamical order-parameter correlation function shows the softening of the damped phonon-like modes as T approaches T_c and the formation of a central peak at T_c, consistent with the presence of soliton-like excitations. For small $|T-T_c|$ an additional broad peak appears at low frequencies. This is interpreted as an additional phonon-like peak, the two quasi-phonon processes being associated with vibration across the potential barrier and vibration in one or other of the two potential wells respectively. Although the squared frequency ω_s^2 of the soft quasi-phonon is approximately linear with $|T-T_c|$ over a range of temperatures, as T increases the ω_s^2 curve eventually flattens out.

1. Introduction

Information concerning the correlation properties of structural phase transitions may be obtained through observation of diffuse X-ray and neutron scattering. Spatial correlations are derivable from the widths in reciprocal space of diffuse peaks, the peaks in some cases becoming superlattice Bragg reflections as the temperature T drops to T_c and below (see e.g. Henriques *et al.* 1984). For the case of neutron scattering, energy analysis of the inelastic intensity allows time-dependent correlations of the system to be observed in frequency space. Such results have shown the softening of certain phonon frequencies to be associated with some structural phase transitions (e.g. in $KMnF_3$, Gesi *et al.* 1972) and the appearance of a central peak in the dynamical response function at temperatures near T_c has also sometimes been observed [Riste *et al.* (1971) made the first such observation in $SrTiO_3$]. This central peak corresponds to an excitation of the system with a very long characteristic timescale compared with that of the phonons and, although it could be caused by extrinsic phenomena, such as structural defects, an alternative purely anharmonic cause is the slow movement of domain walls across the crystal (i.e. a soliton-like excitation). The central peak arising from such propagating walls has been computed for a one-dimensional coupled double-well model by Aubry (1976) (see also Aubry 1975; Krumhansl and Schrieffer

0004-9506/87/050619$02.00

1975). For two-dimensional systems also, MD calculations by Schneider and Stoll (1976), Kerr (1979) and Kerr and Bishop (1986) have shown that the central peak can arise as a purely anharmonic feature associated with soliton-like excitations of the system. Softening of the phonon driving the transition also occurs as an accompanying feature.

All of the above models have been based upon a coupled *quartic* multiple-well potential, which may be a reasonable model for some systems near T_c, but gives a nonlinear temperature dependence for the mean-square displacement (MSD) for $T \gg T_c$. This is at variance with experimental MSD data for the soft-mode systems K_2SnCl_6 (Mair 1984) and $CsPbCl_3$ and $CsPbBr_3$ (Sakata *et al.* 1980), which show that the MSD of the halide ion, which is the ordering species, is linear with temperature at temperatures well above T_c. A multiple-well potential with quadratic walls gives the experimentally observed linear behaviour for the MSD at high temperatures. This has been shown for a range of harmonically coupled quadruple-quadratic potentials by Mair (1986) using MD for a two-dimensional lattice of particles (and for the one-dimensional case by Mair 1983*a*, 1983*b*).

In $SrTiO_3$ (Ivanov *et al.* 1979) the MSD departs from linearity several hundred degrees above the phase transition, the approximate form for the MSD being $cT + dT^2$, where c and d are positive and $d \ll c$. This temperature dependence is typical of many substances at high temperature and would be consistent with the addition of a small *negative* quartic term to the quadratic-walled potential, allowing the walls to become 'softer'. A quartic multiple-well potential, by contrast, has walls that are even 'harder' than quadratic.

In the present paper, one of the quadruple-quadratic models of Mair (1986), with an anti-ferrodistortive structural phase transition, is adopted for calculation of the space and time dependent correlation properties. As the quadruple-quadratic potential has a cusp-shaped barrier, a modification with a smoothed barrier is also considered. MD results for the pair-displacement correlations as a function of particle separation and temperature are presented and compared with results for one-dimensional systems and the two-dimensional Ising model. The frequency spectrum for the time dependent order-parameter correlation function is also calculated for a range of temperatures and the results compared with those for the quartic models mentioned above. Diagrams are presented showing the time evolution of ordered clusters.

2. Definitions and Equations

The details of the model and numerical methods are treated in Mair (1986) (model 1B of that paper is the one used here), so only an outline of these will be given here.

(a) Methods

The vibrational potential Φ is written in terms of the displacements (x_{lk}, y_{lk}) of the atoms from their high temperature phase equilibrium positions, defined by the intersections (l, k) of a square grid. Here Φ is the sum of an effective one-particle potential ϕ_{anh} and a harmonic nearest-neighbour coupling component ϕ_c:

$$\Phi = \phi_{anh} + \phi_c , \tag{1}$$

where

$$\phi_c = \sum_{lk} [\tfrac{1}{2} m\omega_c^2 \{(x_{lk}-x_{l+1\,k})^2+(y_{lk}-y_{lk+1})^2 + (x_{lk}-x_{lk+1})^2+(y_{lk}-y_{l+1\,k})^2\} + \tfrac{1}{2} m\omega_d^2 \{(x_{lk}-y_{l+1\,k})^2+(y_{lk}-x_{l+1\,k})^2 + (x_{lk}-y_{lk+1})^2+(y_{lk}-x_{lk+1})^2\}], \quad (2)$$

and

$$\phi_{anh} = \sum_{lk} \{f(x_{lk})+f(y_{lk})\}, \quad (3a)$$

where

$$f(u) = \tfrac{1}{2} m\omega_0^2(|u|-d)^2. \quad (3b)$$

Choosing numerical values (scaled to unit mass and lattice constant) for the parameters in (1) to (3) of $m\omega_0^2 = 4{\cdot}0$, $d = 0{\cdot}1$, $m\omega_c^2 = -0{\cdot}1$ and $m\omega_d^2 = 1{\cdot}0$, the potential Φ has its two deep minima in the directions $\langle 1\,-1\rangle$ and $\langle -1\,1\rangle$. An anti-ferrodistortive phase transition occurs at temperature $T_c = 0{\cdot}029$ (scaled by the inverse Boltzmann constant), the soft-mode driving the phase transition having wave vector $\boldsymbol{q}_s = (\pi/a_0)(\boldsymbol{e}_1+\boldsymbol{e}_2)$, where a_0 is the lattice constant and $\boldsymbol{e}_1$ and $\boldsymbol{e}_2$ are unit vectors directed along the x and y axes defining the square grid [Fig. 1 of Mair (1986) shows the displacements of the atoms in going from the high to the low temperature phases].

For the case where the cusped barrier in ϕ_{anh} is smoothed, we redefine $f(x)$ in (3a) over the region $|x| < d/4$ by

$$f(x) = ax^6/d^4 + bx^4/d^2 + cd^2 \quad (4)$$

and analogously for the $f(y)$ in (3a) over the region $|y| < d/4$. Choosing $a = 426{\cdot}667$, $b = -64$ and $c = 0{\cdot}708333$ ensures that ϕ_{anh} is smooth everywhere. Retaining the ϕ_c of (2), a completely similar anti-ferrodistortive phase transition occurs for this modified potential, except that T_c is marginally smaller.

(b) MD Calculations

The MD method, which was first used for calculations on fluids (Alder and Wainwright 1960; Rahman 1964), involves the numerical solution of the equations of motion for the velocities and displacements of the particles at successive time intervals. In the present work the calculations were performed on a CYBER 205 computer, extensive use being made of vector processing. The number of particles was N^2, where $N = 40$ for the unmodified potential of equations (1)–(3) and $N = 20$ for the modification of (4). Periodic boundary conditions were employed. The temperature was fixed by scaling the mean-square velocity of the particles to the desired value at each time-step. The time-step was fixed at $0{\cdot}01$ (the unit of time being inversely related to the frequency units). The number of time-steps to achieve stabilisation and then to obtain the required averages varied somewhat with the temperature and with the quantity being estimated. The largest number of time-steps were required near T_c (e.g. 5×10^5 at $T = 0{\cdot}030$), where the timescale for variation of the system is

long. Time averages were taken over a minimum of 10^5 and a maximum of 4×10^5 time-steps.

Ensemble averages were carried out assuming ergodicity. In general, for the quantity X, with value $X_i(t)$ for the ith atom at the tth time-step, the average was calculated as

$$\langle X\rangle = N^{-2}n(t_F, t_I)^{-1}\sum_{t=t_I}^{t_F}\sum_{i=1}^{N^2}X_i(t), \tag{5}$$

where $n(t_F, t_I)$ is the number of time-steps in the interval $t_F - t_I$. For the time-averaged x component of the order parameter $\langle S_x\rangle$, the spatial average in (5) takes the form

$$S_x(t) = N^{-2}\sum_{lk}(-1)^{l+k}x_{lk}(t), \tag{6}$$

the y component being, by symmetry of the equations of motion, equal but opposite in sign [see Fig. 1*a* of Mair (1986) for a diagram of the ordered structure].

For two-particle properties, the spatial average is over all pairs of particles. Then for the correlation function Γ_i, which is the pair-displacement correlation normalised by the MSD, $\langle x^2\rangle$, we have

$$\langle x^2\rangle\Gamma_i = n(t_F, t_I)^{-1}N^{-4}\sum_{t=t_I}^{t_F}\sum_{j=1}^{N^2}\sum_{k=1}^{N^2}x_{jk}(t)\,x_{j+i,k+i}(t) \tag{7}$$

for the $\langle 11\rangle$ direction. For $N = 40$ and periodic boundary conditions, the calculations were made for $i = 1$ to 19. To obtain a better estimate for Γ_i, the mean value of (7) and the corresponding y component was taken. The two components should be equal by symmetry.

(c) Time and Frequency Dependent Properties

We now define the atomic displacement $\boldsymbol{u}_{lk}(t)$, referred to the mean positions $\boldsymbol{R}_{lk}$ of the equilibrium phase. Above T_c, $u_{lk}(t)$ has cartesian components $(x_{lk}(t), y_{lk}(t))$. Below T_c, the components become

$$(x_{lk}(t)-(-1)^{l+k}\langle S_x\rangle,\ y_{lk}(t)-(-1)^{l+k}\langle S_y\rangle),$$

and these components are still valid above T_c as $\langle S_x\rangle$ and $\langle S_y\rangle$ are then zero.

The Fourier amplitudes of the $\boldsymbol{u}_{lk}(t)$ are defined as

$$\boldsymbol{u}(\boldsymbol{q}, t) = \sum_{lk}\boldsymbol{u}_{lk}(t)\exp(-\mathrm{i}\,\boldsymbol{q}\cdot\boldsymbol{R}_{lk}).$$

The wave-vector dependent correlation function may then be defined (see also Kerr 1979) as

$$D(\boldsymbol{q}, t) = N^{-4}\langle\boldsymbol{u}(\boldsymbol{q}, t+t')\cdot\boldsymbol{u}(-\boldsymbol{q}, t')\rangle_{t'},$$

where $\langle\ldots\rangle_{t'}$ denotes an average over time only. For the special case of the wave vector $\boldsymbol{q}_s$, the correlation function $D(\boldsymbol{q}_s, t)$ [hereafter referred to as the dynamical order-parameter correlation function $D(t)$] reduces to

$$D(t) = 2\{n(t_F - t, t_I)\}^{-1}\sum_{t'=t_I}^{t_F}\{S_x(t+t')-\langle S_x\rangle\}\{S_x(t')-\langle S_x\rangle\}. \tag{8}$$

In the present calculations $D(t)$ is normalised to $D(0)$.

The corresponding frequency spectrum is defined as

$$D(\omega) = \int_{-\infty}^{\infty} D(t) \exp(\mathrm{i}\,\omega t)\,\mathrm{d}t,$$

and was evaluated as

$$D(\omega) = \Delta t \sum_{t=t_\mathrm{I}}^{t_\mathrm{F}} D(t) \cos(\omega t) A(t), \tag{9}$$

where $A(t)$ is a gaussian function chosen primarily to damp out the values of t near t_F, which are not reliable because of insufficient averaging in (8). More explicitly, we have

$$A(t) = \exp(-\alpha t^2),$$

with α being chosen so that $A(\frac{1}{2}(t_\mathrm{F} - t_\mathrm{I})) = \frac{1}{2}$. The function $A(t)$ also partially smooths out the step-function aperture for $D(t)$, caused by the finite time interval in (9), so that $D(\omega)$ does not oscillate to strongly negative values. The position of the peaks in $D(\omega)$ is insensitive to the presence of $D(t)$ in (9). Since the time averages for $D(t)$ were over very long times, the width of $A(t)$ could be chosen to be large enough to have negligible effect on the widths of the peaks of $D(\omega)$.

The frequency spectrum $D(\omega)$ is closely related to the cross section for neutron inelastic scattering (see e.g. Marshall and Lovesey 1971) at wave vector $\boldsymbol{q} = \boldsymbol{q}_\mathrm{s}$, if we assume the one-phonon approximation.

3. Results

Before presenting the results for the pair-displacement correlations and the order-parameter spectral function it is useful to consider the MSD. There are two reasons for this; firstly, the effect of modification of the potential barrier can be demonstrated and secondly, the MSD provides a useful framework for interpreting the physical processes that are occurring.

(a) Mean-square Displacement

The MSD is represented in Fig. 1 for the potential with and without the smoothed barrier. In Mair (1986) it was shown that the size effect on the MSD is negligible for $N > 16$, so that any differences in the sets of points in Fig. 1 are truly due to the shape of the potential barrier. It is clear that the cusp-shaped potential barrier does not cause any anomalous effects in the MSD, as the two sets of results are so similar. The largest deviations occur near T_c, and are mainly attributable to the lowering of the barrier through smoothing. For a more extensively modified barrier, the deviations are similar but larger (see Mair 1986).

The physical interpretation of the shape of the MSD is as follows. In the linear region for $T < 0{\cdot}015$ the particles are vibrating in either of the two deep potential wells, but are not sufficiently energetic to hop across the potential barrier. The MSD then corresponds to harmonic motion about one or other of the two sites defined by the deep minima in the potential, each site being occupied with equal probability.

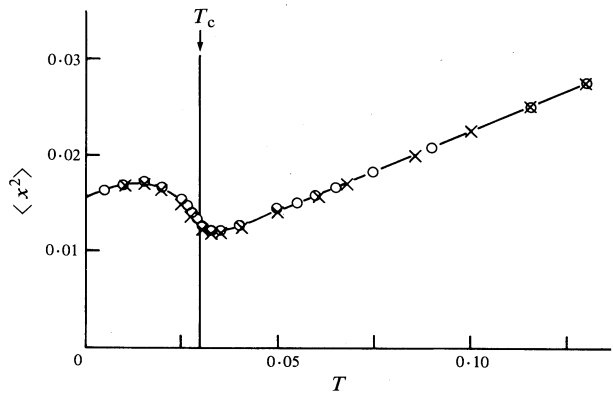

Fig. 1. MSD $\langle x^2 \rangle$ ($=\langle y^2 \rangle$) as a function of scaled temperature, with displacements being taken with respect to the equilibrium positions for the high temperature phase. The open circles are for the unmodified potential of equations (1)–(3) and the crosses are for the potential with the smoothed barrier. In this and all other figures the curve through the points is only a guide to the eye.

In the region $0{\cdot}015 \leqslant T \leqslant 0{\cdot}065$ there is a dip in the MSD. This is the region in which there are two competing effects: (a) vibration about one or other of the 'sites' defined by the potential minima, as for $T < 0{\cdot}015$, and (b) hopping across the potential barrier, which is now energetically possible. As the temperature is raised above about $0{\cdot}065$ the presence of the potential barrier becomes insignificant and effect (b) becomes the dominant one. The MSD has by then recovered its value before going through the dip and the quadratic walls of the potential cause the MSD to increase linearly once again.

The gradients $\mathrm{d}\langle x^2 \rangle / \mathrm{d}T$ at high and very low temperatures are the same and are determined by the quadratic one and two particle potential parameters. A more general choice of potential barrier, such as a sextic polynomial for $|x| < d$ (rather than for $|x| < d/4$ as in equation 9), causes the high and low temperature gradients to differ (see Mair 1986) as the sextic polynomial parameters influence the shape of the potential at low but not high energies.

Note that the high temperature MSD extrapolates linearly to a nonzero value at $T = 0$. This value is determined by d'^2, where d' is the separation in the potential minima of the high temperature effective one particle potential, and $d' < d$. This may be more clearly understood by reference to Mair (1983*b*), where effective one particle potentials were calculated for a series of double-quadratic chains (see particularly Fig. 7 of that reference).

(b) Pair-displacement Correlations

All calculations of the pair-displacement correlations Γ_j were carried out on the potential with the unmodified barrier.

The pair-displacement correlations, similar to the MSDs, vary smoothly with temperature through T_c. As shown in Fig. 2, a steep rise in the Γ_j occurs near T_c as the temperature is lowered. This is a direct result of the greatly increased correlation across the crystal as the particles become ordered. The rise in Γ_j is more pronounced

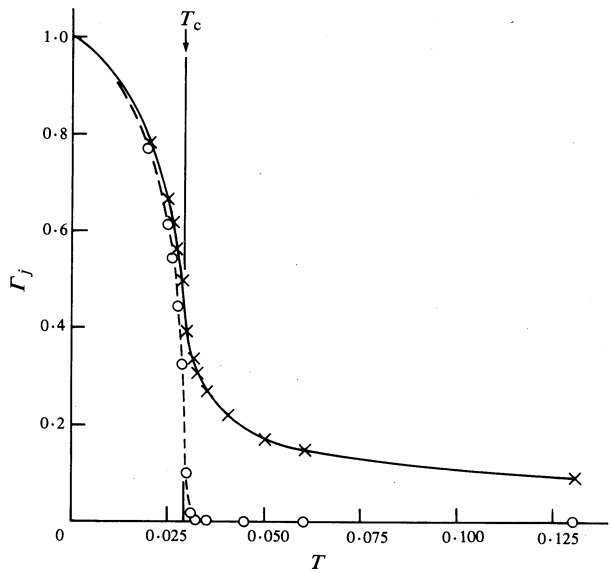

Fig. 2. Pair-displacement correlations for first (crosses) and tenth (circles) neighbours (Γ_1 and Γ_{10}) in the direction $\langle 11 \rangle$, as a function of scaled temperature.

for the pair-displacement correlations at large separation (compare $j = 1$ and $j = 10$ in Fig. 2). As the temperature increases, Γ_j tends to a constant, indicating that the $\langle x_{jk}\, x_{j+i,k+i} \rangle$ vary linearly with temperature, similar to the MSDs.

The dependence of Γ_j upon the particle separation j is illustrated in Fig. 3. The logarithmic plot in Fig. 3*a* shows that, unlike the one-dimensional case of a chain of particles (Johnson and Mair 1985), the pair-displacement correlations do not decay exponentially with distance, although for the highest temperatures the curves become more nearly exponential. Well below T_c, the Γ_j are almost constant with j, a result of the long-range ordering. In fact, with increase in j the Γ_j tend to $\langle S_x \rangle^2 / \langle x^2 \rangle$. In order to see the effect of the fluctuation in Γ_j for $T < T_c$, it is necessary to subtract out this ordering component, and so we define

$$\Gamma_j' = \Gamma_j - \langle S_x \rangle^2 / \langle x^2 \rangle. \tag{10}$$

Asymptotic expansions of the spin–spin correlation in the two-dimensional Ising model (Kadanoff 1966), which is a magnetic analogue of the present system, have shown that for large separations r, and T above but near T_c, the spin correlation function varies as $r^{-1/2} \exp(-\lambda r)$, where λ is independent of r. The parameter λ may be considered to be an inverse correlation length for the system. For $T < T_c$ Kadanoff found that the fluctuation in the spin correlations varies as $r^{-2} \exp(-2\lambda r)$ for large r, and quoted a variation proportional to $r^{-1/4}$ for $r \to 0$.

Logarithmic plots of $j^{1/2} \Gamma_j'$ against j for T near T_c are presented in Fig. 3*b* for $j \leqslant 10$. The functions are not plotted for larger j as the generally very small values of Γ_j' for j large could not be computed reliably enough. The linearity of the plots for T near T_c (i.e. at $T = 0{\cdot}030$ and $0{\cdot}02875$) shows that, for distances up to one-quarter of the diagonal length of the crystal, Γ_j' varies as $r^{-1/2} \exp(-\lambda r)$ for this system,

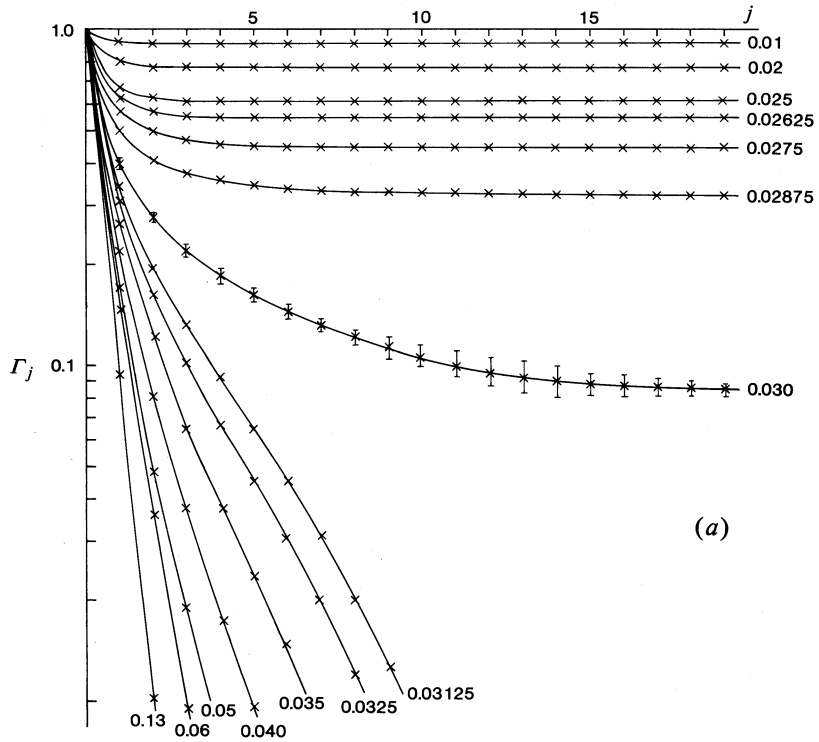

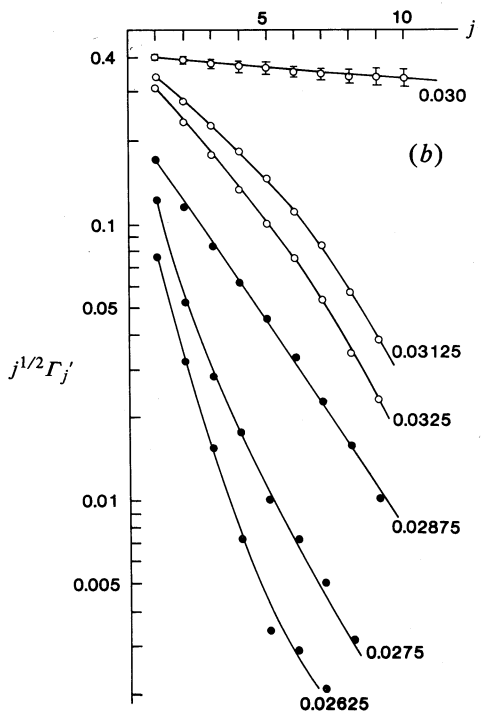

Fig. 3.
(*a*) Pair-displacement correlations in the direction ⟨11⟩ as a function of separation, the Γ_j being plotted on a logarithmic scale. Curves are marked with the scaled temperature. The error bars for $T = 0{\cdot}030$, derived from successive calculations, are indicative of that type of error at the other temperatures.
(*b*) Logarithmic plots of $j^{1/2}\Gamma_j'$ as a function of separation j. The Γ_j' are the same as Γ_j of Fig. 3*a* for $T > T_c$ (open circles), but for $T < T_c$ the long-range order component has been subtracted out (closed cicles). Curves are marked with the scaled temperature.

not only above but also below T_c. The low gradient of the curve at $T = 0{\cdot}030$ indicates a long correlation length, as expected near T_c. As $|T - T_c|$ increases the gradients at low j also increase in size, corresponding to a decrease in correlation length, and the nonlinearity of the curves shows the $r^{-1/2}\exp(-\lambda r)$ relationship to be less appropriate. Note that neither of the Ising model predictions quoted above for $T \leqslant T_c$ are obeyed by the present system.

(c) Dynamical Order-parameter Correlations

Examples of the frequency spectrum for the order-parameter correlation function (equations 8 and 9) are presented in Fig. 4. In most cases, several repetitions of the calculations were carried out to assess the reliability of the results. The spectra show the soft-phonon mode peaks (at frequency ω_s) and, as shown in Fig. 4*i*, there is also a second mode at scaled frequency $\omega_o \sim 3{\cdot}1$. The spectra shown in Figs 4*a*–4*h* have not been extended out far enough in ω to show this peak. The spectra show oscillations due to the finite time interval for averaging and are not highly reproducible near T_c, particularly near $T = 0{\cdot}04$. Splitting of the peaks also tends to occur in this temperature region, especially for shorter averaging times. [Compare the small broad peak in Fig. 4*e* near $\omega = 0{\cdot}7$ with the multiple peaks in the same frequency range in Fig. 4*f*. Fig. 4*e* is calculated for 4×10^5 time-steps (4000 time-units), twice the time used for Fig. 4*f*.] An estimate of the resolution in ω is provided by the full width at half height $\Delta\omega$ of the phonon peaks in $D(\omega)$ for the harmonic model, obtained for $d = 0$ in equation (3b). MD calculations give $\Delta\omega = 0{\cdot}04$ for this case.

The general features evident from the spectra are as follows. At $T = 0{\cdot}02$ there is a rather broad peak, corresponding to the damped phonon-like mode at $\omega_s \approx 1{\cdot}1$, but no other feature. [An exception is the small, somewhat sharper peak at $\omega_o = 3{\cdot}27$, with peak height $D(\omega_o) = 1{\cdot}85$, corresponding to the optic mode at the same wave vector. This occurs beyond the frequency range of the diagram.] As T is raised to $0{\cdot}025$ the quasi-phonon frequency decreases (i.e. softens) and a new, broad feature occurs below $\omega \sim 0{\cdot}3$. By $T = 0{\cdot}0275$ the latter feature overlaps with a much more intense peak centred very near $\omega = 0$. At the same time the quasi-phonon mode appears to have softened further, to $\omega_s \sim 0{\cdot}3$, although there is no clear delineation between the quasi-phonon peak and the feature near $\omega = 0$. At $T = 0{\cdot}03$, which is just above T_c, there is only a single narrow peak centred on $\omega = 0$, corresponding to an almost stationary value of the order parameter and consistent with 'soliton' like excitations. At $T = 0{\cdot}04$ there is again a broad additional peak at a small finite frequency, overlapping a much-reduced central peak. A rather broad quasi-phonon peak, near $\omega \sim 0{\cdot}7$ in Fig. 4*e*, can now be distinguished, although there is considerable uncertainty in its exact position. By $T = 0{\cdot}06$ this quasi-phonon peak is again well defined, the central peak has disappeared and the broad extra peak at low frequency is reduced in intensity. This feature has almost disappeared by $T = 0{\cdot}065$ and the quasi-phonon frequency has again increased, until at $T = 0{\cdot}13$ a value of $1{\cdot}1$ is reached. Note that an extra peak in $D(\omega)$ has also been observed by Kerr (1979), but only in a narrow range of temperatures above T_c (certainly not at $2T_c$ as obtained here) and always accompanied by a central peak.

The spectra are not sufficiently well defined to give good quantitative data on quasi-phonon lifetimes and central peak widths. However, it is clear that the

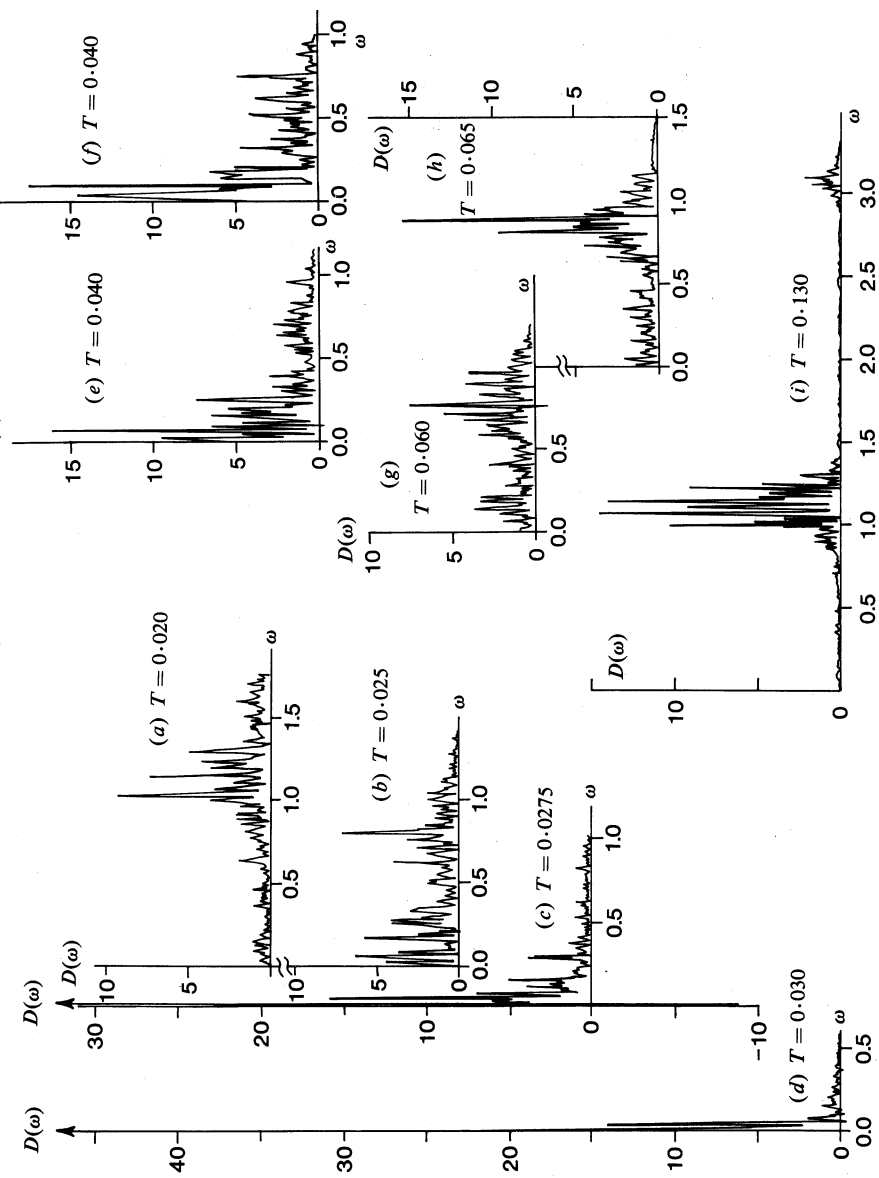

Fig. 4. Representative frequency spectra for the order-parameter correlation function $D(\omega)$, for scaled temperatures as marked. All spectra are for the unmodified potential of equations (1)–(3). For (*c*) and (*d*) the highest peak of $D(\omega)$ extends beyond the scale of the figure. The frequency range for (*i*) is extended to show the optic mode peak at ω_0.

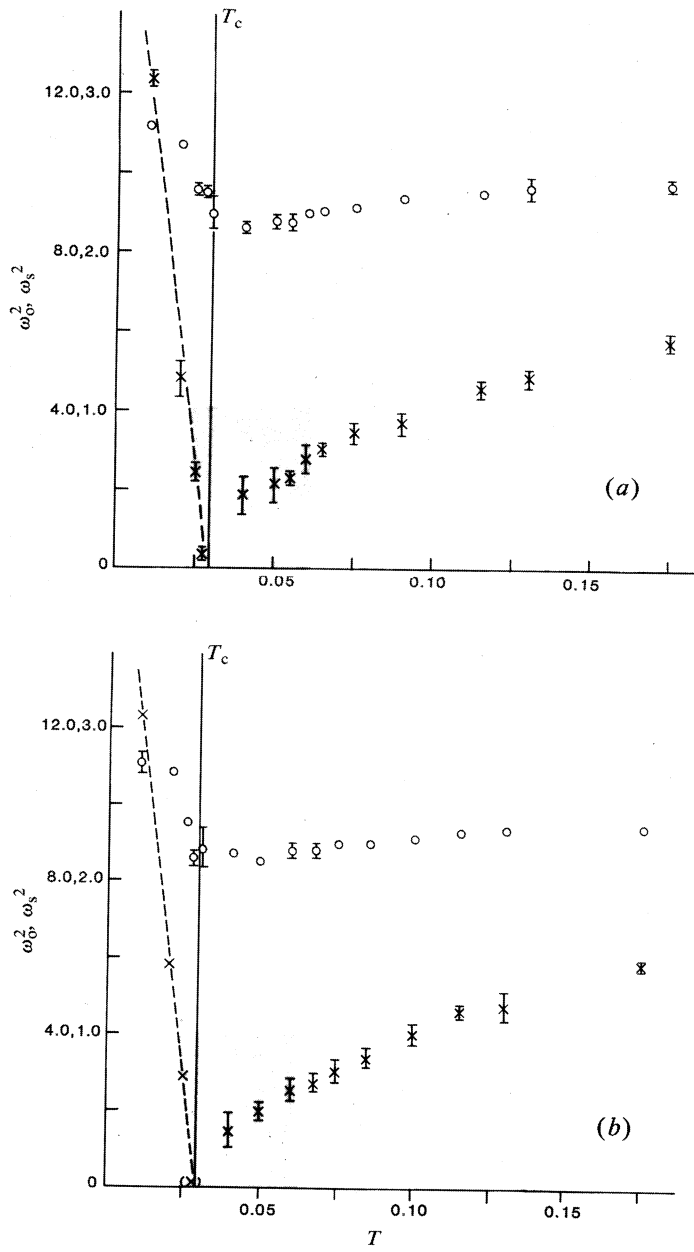

Fig. 5. Square of the soft-mode frequency ω_s^2 (crosses) as a function of scaled temperature for (*a*) the unmodified potential and (*b*) the potential with the smoothed barrier. The open circles are the squared frequencies ω_o^2 for the optic mode occurring at the same wave vector (see Fig. 4*i*). Note that ω_o^2 is much larger than ω_s^2 and is plotted on a different scale. Error bars, where present, are derived from repeated calculations and from uncertainties in the peak position due to poor definition of its shape. The dashed line corresponds to the Curie–Weiss law for $T < T_c$. The shading is discussed in Section 4*c*.

soft-phonon peak half-widths increase as T decreases towards T_c, corresponding to a decrease in phonon lifetime, and that the central peak width at T_c is very narrow, representing long-lived excitations of the system.

The results for the quasi-phonon frequencies ω_s and ω_o are summarised in Fig. 5*a*, where ω_s^2 and ω_o^2 are plotted as a function of temperature. Estimates of ω_s and ω_o were made from the mean peak positions of two to five calculations of $D(\omega)$. Fig. 5*b* shows corresponding data for the potential with the smoothed barrier. The result for ω_s^2 at 0·0275 is placed in parentheses, since it is not clear that a quasi-phonon can be unambiguously separated out from the spectrum at this temperature.

Figs 5*a* and 5*b* are almost the same within error, so that it may be concluded that the cusped barrier for Fig. 5*a* does not have a significant effect on the essential features of the T dependence of the frequencies. Both figures show that the optic mode softens as T_c is approached from above or below, a rather steep change in ω_o^2 occurring below T_c. The squared soft-mode frequency ω_s^2 appears to obey the Curie–Weiss law below T_c, with ω_s going to zero at T_c if the datum-point at $T = 0{\cdot}0275$ can be relied upon. Immediately above T_c the uncertainty in peak position means that the temperature dependence is not known. Certainly, a linear dependence on $T - T_c$ does not exist over the complete temperature range above T_c. The results show that the ω_s^2 curve is gradually flattening out as T increases, although it is approximately linear in the range $0{\cdot}06 < T < 0{\cdot}115$.

Since Fig. 5*b* was calculated for a lattice of 400 particles, whereas 1600 were used for Fig. 5*a*, finite size effects appear to be minimal. This conclusion also applies to the $D(\omega)$ which are very similar for both sizes of lattice.

(d) Motion of Clusters

Although the appearance of the central peak in $D(\omega)$ is consistent with the presence of soliton-like excitations, more direct evidence of such excitations is given by plots of the evolution of the system in space and time concurrently. In Figs 6*a* and 6*b* the time evolution of the 40 particles in a row of the lattice is traced for $T = 0{\cdot}030$ and 0·025 respectively. The dark portions of the diagrams represent regions where the local order parameter is negative, the remaining areas corresponding to positive local order parameter. At $T = 0{\cdot}030$, we see evidence of large clusters with very long lifetimes. The border between the major black and white regions is almost parallel to the time axis, indicating that the velocity component of the cluster wall along the row is almost zero. These features are the signatures for a soliton-like excitation with a central peak in the frequency spectrum.

At $T = 0{\cdot}025$, the system is fairly well ordered but still contains clusters of the opposite sign. Fig. 6*b* shows that some of these clusters still have a considerable lifetime, but are much shorter lived than at $T = 0{\cdot}030$. The boundaries of the larger dark portions of Fig. 6*b* are not parallel to the time axis, indicating that the cluster walls have finite velocities along the row.

Similar effects to these have been observed by Schneider and Stoll (1976), who also found a new branch in the dispersion surface in the vicinity of the critical wave vector. They suggested that the 'cluster waves' (i.e. soliton-like excitations) are responsible for this new branch.

Note that a small contribution to the central peak will also result from relaxational hopping.

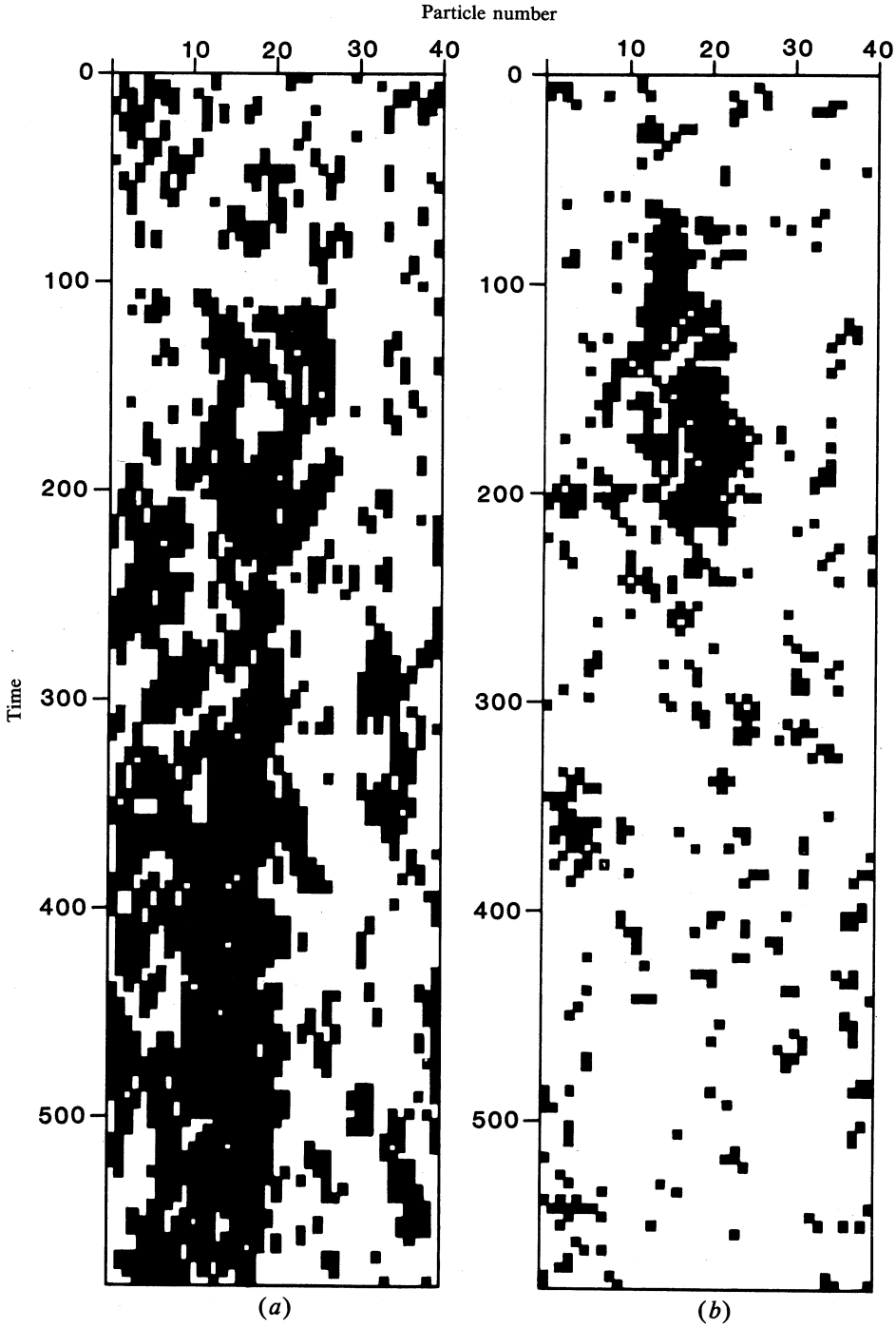

Fig. 6. Variation of the sign of the local order parameter with time for a row along the x direction of the lattice at scaled temperatures of (*a*) 0·030 and (*b*) 0·025. Dark (light) regions correspond to negative (positive) local order parameter. Note that the timescale is in units of scaled time, not time-steps (see Section 2 *b*).

4. Discussion

(a) Pair-displacement Correlations

The pair-displacement correlations $\Gamma(r)$ are unlike the MSDs (Mair 1986) in that they are highly dependent on the dimensionality of the system. A good example of this is shown by comparing the $\Gamma(r)$ across and along the chains in a two-dimensional model crystal composed of weakly coupled chains (Kerr and Bishop 1986). These results show that $\Gamma(r)$ along the chains is exponential with r, and thus one dimensional in character, whereas perpendicular to the chains $\Gamma(r)$ is not exponential [the detailed form of $\Gamma(r)$ perpendicular to the chains was not analysed].

The increase in the correlation length with decrease in temperature, evident from the Γ curves of Fig. 3*a*, also appears as a decrease in width in the diffuse and (for $T < T_c$) superlattice peaks in the coherent X-ray scattering. This effect was illustrated by Mair *et al.* (1987), who have calculated coherent X-ray scattering intensities over a range of temperatures for the present model. Since the intensity of first-order diffuse scattering is proportional to the pair correlations $\langle x_{jk}\, x_{j+i,k+i}\rangle$ (see Borie 1970), the present model predicts approximately linear high temperature behaviour for this component of the scattered intensity.

(b) Mode Softening

Although there is much experimental evidence that soft-mode frequencies obey the Curie–Weiss law at temperatures well above T_c, a clear case of the flattening of the ω_s^2 temperature curve is given by the infrared data for $SrTiO_3$ by Servonin *et al.* (1980). This deviation from the Curie–Weiss law is found in the present MD results, but is not observed in the MD results of Kerr (1979) or Kerr and Bishop (1986), who used quartic multiple-well potentials. Recalling that for a harmonic system ω is independent of temperature, the flattening of the ω_s^2 temperature curve may be understood as a tendency towards less anharmonic behaviour as temperature increases. At very high temperatures the quadratic multiple-well potential behaves increasingly like a single harmonic well, whereas a quartic multiple-well potential always remains a highly anharmonic system.

(c) Order-parameter Spectral Function near T_c

The order-parameter spectral function outside the region $0{\cdot}025 < T < 0{\cdot}0625$ (shaded in Fig. 5) consists of a well-defined damped phonon-like peak. Within the shaded region an extra, broad peak occurs at low frequencies, the damped phonon-like peak is more poorly defined and, close to T_c, the central peak occurs. This region coincides with the main part of the dip in the MSD curve (see Fig. 1 and Section 3*a*), where competing interactions are occurring, namely hopping across the potential barrier and vibration about one or other of the potential minima. As a result of the spatially correlated nature of these two processes, domain walls and quasi-phonons are formed and interact.

Aubry (1976) has found that for a displacive chain of quartic double wells there are three possible solutions to the equations of motion; a 'soliton' solution, which is stable at all energies and gives rise to the central peak in $D(\omega)$, and two pseudo-phonon solutions, one of which is stable at low energies and the other at higher energies. There is an energy region in which all three of these solutions are stable, producing

a three-peaked structure in $D(\omega)$, i.e. a central peak and two pseudo-phonon peaks. Near T_c this three-peaked structure is just discernible in the spectra of Fig. 4. For slightly larger $|T-T_c|$, the central peak disappears and *two* broad peaks remain, the extra peak persisting to $2T_c$. Three-peaked structure in $D(\omega)$ was also observed in the MD results of Kerr (1979), but only up to $\sim 1{\cdot}2T_c$, and no very clear interpretation of the physical processes causing the extra low-frequency peak was given.

The results of Aubry apply for a one-dimensional case of quartic double wells, but it seems likely that analogous processes would occur in the present two-dimensional system. Then the two peaks in $D(\omega)$ at nonzero ω would both be interpreted as *phonon-like excitations* due to the two competing processes (a) correlated hopping across the barrier and (b) correlated vibration in one or other of the potential wells. Process (a) becomes energetically unfavourable at low temperatures and (b) at high temperatures, corresponding to the observed appearance of only a single peak in $D(\omega)$ at very low and high temperatures. In the region of their co-existence, the quasi-phonons and the 'solitons' interact, causing the observed poor definition and broadening of the quasi-phonon peaks near T_c.

5. Conclusions

The main conclusions arising from this MD study on the system described are as follows:

(1) The fluctuation in the pair-displacement correlations $\Gamma'(r)$ varies with distance as $r^{-1/2}\exp(-\lambda r)$ for $|T-T_c|$ small and for distances at least out to the tenth neighbour in the 40×40 particle lattice.

(2) The squared soft-mode frequency varies less strongly than T as temperature T increases.

(3) A central peak is observed in the order-parameter frequency spectrum. This is consistent with the presence of soliton-like excitations whose existence has been demonstrated by diagrams of the time evolution of a row of the lattice.

(4) For a small region near T_c, it is postulated that two competing quasi-phonon modes exist, one corresponding to vibration across the potential barrier and the other to vibration within one or other of the potential wells. Taken with the central peak, these modes give rise to a three-peaked structure in the time dependent order-parameter frequency spectrum at $T \sim T_c$, and a two-peaked structure for slightly larger $|T-T_c|$.

Acknowledgments

I wish to thank Dr C. H. J. Johnson for many useful discussions on the computing and Dr S. W. Wilkins for a critical reading of the manuscript. The work was carried out with the support of a CSIRO Cyber 205 Grant.

References

Alder, B. J., and Wainwright, T. E. (1960). *J. Chem. Phys.* **33**, 1439–51.
Aubry, S. (1975). *J. Chem. Phys.* **62**, 3217–29.
Aubry, S. (1976). *J. Chem. Phys.* **64**, 3392–402.
Borie, B. (1970). *Acta Crystallogr.* A **26**, 533–5.
Gesi, K., Axe, J. D., Shirane, G., and Linz, A. (1972). *Phys. Rev.* B **5**, 1933–41.

Henriques, R. T., Alcacer, L., Pouget, J. P., and Jerome, D. (1984). *J. Phys.* C **17**, 5197–208.
Ivanov, S. A., Mikal'chenko, V. P., and Venevtsev, Yu. N. (1979). *Dokl. Akad. Nauk SSSR* **284**, 865–7.
Johnson, C. H. J., and Mair, S. L. (1985). *J. Phys.* C **18**, 67–75.
Kadanoff, L. P. (1966). *Nuovo Cimento* **44** B, 276–305.
Kerr, W. C. (1979). *Phys. Rev.* B **19**, 5773–802.
Kerr, W. C., and Bishop, A. R. (1986). *Phys. Rev.* B **34**, 6295–314.
Krumhansl, J. A., and Schrieffer, J. R. (1975). *Phys. Rev.* B **11**, 3535–45.
Mair, S. L. (1983*a*). *J. Phys.* C **16**, 4811–25.
Mair, S. L. (1983*b*). *J. Phys.* C **16**, 5591–604.
Mair, S. L. (1984). *Solid State Commun.* **52**, 335–7.
Mair, S. L. (1986). *J. Phys.* C **19**, 6321–38.
Mair, S. L., Johnson, C. H. J., and Lynch, D. F. (1987). *Acta Crystallogr.* A **43** (in press).
Marshall, W., and Lovesey, S. W. (1971). 'Theory of Thermal Neutron Scattering' (Clarendon: Oxford).
Rahman, A. (1964). *Phys. Rev.* **136**, A405–11.
Riste, T., Samuelson, E. J., Otnes, K., and Feder, J. (1971). *Solid State Commun.* **9**, 1455.
Sakata, M., Harada, J., Cooper, M. J., and Rouse, K. D. (1980). *Acta Crystallogr.* A **36**, 7–15.
Schneider, T., and Stoll, E. (1976). *Phys. Rev.* B **13**, 1216–37.
Servonin, J. L., Luspin, Y., and Gervais, F. (1980). *Phys. Rev.* B **22**, 5501–6.

Manuscript received 25 March, accepted 2 July 1987